Auger branching ratios for berylliumlike $1s2s2p^2\,{}^1S,{}^1P,{}^1D$ resonances and photoionization of beryllium from $1s^22s2p\,{}^1P^o$

Wei Cheng Shiu,[1] Chen-Shiung Hsue,[1] and Kwong T. Chung[2]
[1]*Department of Physics, National Tsing-Hua University, Hsin-Chu, Taiwan, Republic of China*
[2]*Department of Physics, North Carolina State University, Raleigh, North Carolina 27602*
(Received 17 December 2000; published 16 July 2001)

The photoionization cross section of Be from $1s^22s2p\,{}^1P^o$ is studied with the saddle-point complex-rotation method for photon energies from 23 to 117 eV. A full-core plus correlation wave function is used for the initial states. In the continuum, the energy and width for the singly core-excited Be-like $1s2s2p^2\,{}^1S$, ${}^1P$, and ${}^1D$ states are calculated to high precision for systems with $Z=4$–10. The Auger decay branching ratios of these states are studied to check the spin alignment theory recently proposed by Chung. These results are compared with the available experimental data in the literature.

DOI: 10.1103/PhysRevA.64.022714 PACS number(s): 32.80.Hd, 32.70.Fw, 31.25.Jf, 31.15.Ar

I. INTRODUCTION

In recent years, the advance in synchrotron technology has stimulated much progress in experimental physics. The availability of high-intensity high-energy photon beams has made many new experiments possible. This has generated considerable interest in the study of hollow atoms, especially the hollow lithium atom [1–7]. Since beryllium is the next element in the periodic table after lithium, it is conceivable that many new synchrotron experiments on beryllium will be carried out in the near future. The available theoretical information in the literature will certainly help experimental workers in their future data analysis.

Our interest in this beryllium study is also stimulated by the experimental work of Meyer *et al.* [8]. In their experiment, the core excited Li $1s2p^2\,{}^2S$, ${}^2P$, and ${}^2D$ states were obtained by first pumping Li atoms with a dye laser

$$1s^22s\,{}^1S+\mathcal{L}(1.848\ \text{eV})\rightarrow 1s^22p\,{}^2P.$$

This is followed by an excitation with synchrotron radiation:

$$1s^22p\,{}^2P+h\nu\rightarrow 1s2p^2.$$

Recently, this technique was again used in the study of even-parity hollow lithium [9]. A generalization of the above process to four-electron systems and the study of the dynamics involved would be of significant interests. In particular, for beryllium we have [10]

$$1s^22s^2\,{}^1S+h\nu(\sim 2349\ \text{Å})\rightarrow 1s^22s2p\,{}^1P^o.$$

A subsequent excitation by synchrotron radiation will lead to the even-parity core-excited beryllium resonances. In this study, we will calculate the energies of these core-excited systems and the corresponding photoionization cross section for

$$1s^22s2p\,{}^1P^o+h\nu\rightarrow 1s2s2p2p({}^1S,\ {}^1P,\ \text{or}\ {}^1D).$$

A detailed study of the energy, width, and excitation cross sections allows us to predict whether these resonances can be observed and the corresponding photon energy required.

To investigate these core-excited resonances, the "saddle-point" method is used [11]. In this approach, spurious solutions are eliminated by directly building the proper vacancy orbitals into the wave functions. The resonances energies and wave functions are obtained by a mini-maxi procedure. The advantage of this method is that a set of optimized basis functions can be found which is relatively compact. This gives an approximated energy from the closed-channel segment. To include the contribution from the open channels, the saddle-point complex-rotation (SPCR) method is employed [12]. The effect of the open channel and the resonance width is calculated with square-integrable basis functions. Finally, using these wave functions, the photoionization cross section can then be obtained [13] following a method suggested by Rescigno and McKoy [14].

Extensive applications of the saddle-point method with and without the complex-rotation method to two- and three-electron systems have been demonstrated [15]. To date, the application of the saddle-point method for four-electron system has been limited to the calculation of energy [16–20]. No SPCR calculation has yet been carried out for systems with more than three electrons. In view of the highly accurate results obtained in the past in two- and three-electron systems, it will be interesting to find out how effective this method will be for widths and photoionization cross sections for four-electron systems.

Recently, a spin-alignment-dependent theory for the Auger decay branching ratios was proposed by Chung [21]. This theory is used to explain the relative branching ratios for the decay of triply excited three-electron systems. It would be interesting to check how this theory works for four-electron systems.

In this work, the following computation procedures are adopted for the core-excited resonances of Be $1s2s2p^2\,{}^1S$, ${}^1P$, and ${}^1D$ and their isoelectronic ions from $Z=4$ to 10.

(i) The energy and the wave function for each resonance are first obtained in the closed-channel with the saddle-point variation method [11] using the nonrelativistic Hamiltonian. This wave function is used to calculate the relativistic corrections.

(ii) The restricted variation method [22] is used to saturate the functional space to further improve the nonrelativistic energy.

(iii) The energy shift due to the interaction of closed-channel segment with the open channels, the Auger decay width, and the photoionization cross section (PICS) are calculated using the complex-rotation method [12,13].

In Sec. II, the theories used are briefly reviewed. The calculated energy and width results are presented in Sec. III. Comparisons with existing experimental data are also given in this section. The results for the photoionization of Be is given in Sec. IV. The last section gives a short conclusion.

II. THEORY

The zeroth-order Hamiltonian for a four-electron system is (in a.u.)

$$H_0=\sum_{i=1}^{4}\left(-\frac{1}{2}\nabla_i^2-\frac{Z}{r_i}\right)+\sum_{i<j}^{4}\frac{1}{r_{ij}}. \tag{1}$$

In this work, the LS coupling scheme will be used. The wave function is a linear combination of configuration interaction (CI) basis functions which are eigenfunctions of L^2, S^2, L_z, and S_z. Here L and S are the total orbital and spin angular momentum of the atom. They may be written as

$$\Phi_{n(i),l(i)}(\mathbf{r}_1,\mathbf{r}_2,\mathbf{r}_3,\mathbf{r}_4)=\varphi_{n(i)}(R)Y_{l(i)}^{LM}(\hat{\mathbf{R}})\chi_{SS_z}, \tag{2}$$

where R represents collectively the radial parts of $\mathbf{r}_1$, $\mathbf{r}_2$, $\mathbf{r}_3$, $\mathbf{r}_4$ and $\hat{\mathbf{R}}$ represents their angular part. The radial parts are products of Slater-type orbitals:

$$\varphi_{n(i)}(R)=\prod_{j=1}^{4} r_j^{n_j}\exp(-\alpha_j r_j). \tag{3}$$

The angular part is given by

$$Y_{l(i)}^{LM}(\hat{\mathbf{R}})=\sum_{m_j}\langle l_1m_1l_2m_2|l_{12}m_{12}\rangle\langle l_{12}m_{12}l_3m_3|l_{123}M_{123}\rangle \times\langle l_{123}m_{123}l_4m_4|LM\rangle\prod_{j=1}^{4}Y_{l_jm_j}(\Omega_j). \tag{4}$$

Here the subscript $l(i)$ denotes the angular coupling:

$$l(i)=[(l_1,l_2)l_{12},l_3]l_{123},l_4. \tag{5}$$

Similarly, the spin angular momentum partial wave for a four-electron system with total spin S and its z component S_z can be represented by

$$\chi_{SS_z}=[(\tfrac{1}{2},\tfrac{1}{2})S_{12},\tfrac{1}{2}]S_{123},\tfrac{1}{2} \tag{6}$$

where the S_{123} and the spin of the last electron ($\frac{1}{2}$) couple into S is implicitly implied. The four-electron spin function χ could either be a quintet ($S=2$), a triplet ($S=1$), or a singlet ($S=0$). In the case of a singlet, two spin angular functions are possible:

$$\chi^1=[(\tfrac{1}{2},\tfrac{1}{2})1,\tfrac{1}{2}]\tfrac{1}{2},0,\qquad \chi^2=[(\tfrac{1}{2},\tfrac{1}{2})0,\tfrac{1}{2}]\tfrac{1}{2},0. \tag{7}$$

In the saddle-point method [11], vacancies are built into the wave function to project out the spurious states. In particular, for the $1s2s2p^2$ resonances considered here, a $1s$ vacancy is built into the total wave function. The wave function is given by

$$\Psi_{LSMS_z}=A\sum_{\substack{l(i)\\n(i)}}C_{n(i)}^{l(i)}(1-P_j)\varphi_{n(i)}Y_{l(i)}^{LM}(\hat{\mathbf{R}})\chi_{SS_z}, \tag{8}$$

where P_j is the projection operator for the $1s$ vacancy orbital:

$$P_j=|\varphi_{1s}(\mathbf{r}_j)\rangle\langle\varphi_{1s}(\mathbf{r}_j)|. \tag{9}$$

In Eq. (8), A is the antisymmetrization operator and $C_{n(i)}^{l(i)}$ are linear coefficients. The vacancy orbital is given by

$$\varphi_{1s}(\mathbf{r}_j)=2q^{3/2}e^{-qr}Y_{00}(\theta,\phi). \tag{10}$$

The optimized value of the parameter q can be interpreted as the effective nuclear charge seen by the vacancy orbital. The linear coefficients C can be determined by solving the secular equation from

$$\delta E_0=\delta\frac{\langle\Psi|H_0|\Psi\rangle}{\langle\Psi|\Psi\rangle}=0. \tag{11}$$

In the saddle-point method, this wave function is obtained by maximizing the nonrelativistic energy E_0 with respect to the parameter q and minimizing E_0 with respect to all other nonlinear parameters α.

The relativistic and mass polarization corrections are obtained by using the first-order perturbation theory. The perturbation Hamiltonians considered here are

$$H'=H_1+H_2+H_3+H_4+H_5, \tag{12}$$

with

$$H_1=-\frac{1}{8c^2}\sum_{i=1}^{4}\mathbf{P}_i^4\quad\text{(correction to kinetic energy)},$$

$$H_2=\frac{Z\pi}{2c^2}\sum_{i=1}^{4}\delta(\mathbf{r}_i)\quad\text{(Darwin term)},$$

$$H_3=-\frac{\pi}{c^2}\sum_{\substack{i,j=1\\i<j}}^{4}\left[1+\frac{8}{3}\mathbf{s}_i\cdot\mathbf{s}_j\right]\delta(\mathbf{r}_{ij})$$

(electron-electron contact term),

$$H_4=-\frac{1}{M}\sum_{\substack{i,j=1\\i<j}}^{4}\boldsymbol{\nabla}_i\cdot\boldsymbol{\nabla}_j\quad\text{(mass polarization)},$$

$$H_5=-\frac{1}{2c^2}\sum_{\substack{i,j=1\\i<j}}^{4}\frac{1}{r_{ij}}\left[\mathbf{P}_i\cdot\mathbf{P}_j+\frac{\mathbf{r}_{ij}(\mathbf{r}_{ij}\cdot\mathbf{P}_i)\cdot\mathbf{P}_j}{r_{ij}^2}\right]$$

(retardation potential),

where M is the nuclear mass and $c=137.036$.

It is well known that the width of a resonance is the result of coupling between the closed- and open-channel components. For a narrow resonance, this coupling is very weak. The resonance wave function can be approximated by the closed-channel component and the resonance energy is largely determined by this component. However, the saddle-point method does not yield the width of a resonance with only the closed-channel segment. On the other hand, the open-channel wave function contains a continuum which is not square integrable in general. In order to handle the open-channel segment with square-integrable basis functions, we follow the SPCR method [12]. We write the N-particle Hamiltonian in the form

$$H(\mathbf{r}_1,\mathbf{r}_2,\ldots,\mathbf{r}_N)=H(R_N,\Omega_N), \tag{13}$$

where R_N represents the set of radial coordinates $r_1,r_2,\ldots,r_N$, and Ω_N represents the corresponding angular coordinates. Using the saddle-point method, an accurate representation of the closed-channel part of the eigenfunction can be expanded in terms of a rather compact basis set $\phi_j(R_N,\Omega_N)$. A complex rotation is now carried out for the Hamiltonian, that is,

$$H=H(R_Ne^{i\theta},\Omega_N), \tag{14}$$

where $R_Ne^{i\theta}$ means that each radial coordinates r_j takes the form $r_je^{i\theta}$. This new Hamiltonian is very different from Eq. (13), and the corresponding eigenfunction is also changed. The eigenvalues along the branch cut varies with θ but the resonant eigenvalue is supposed to be stationary. Note that the nonlinear parameters in ϕ_j which are most suitable for the solution of $H(R_N,\Omega_N)$ may not be suitable for that of $H(R_Ne^{i\theta},\Omega_N)$. However, a corresponding rotation on the basis functions ϕ_j,

$$\phi_j=\phi_j(R_Ne^{i\theta},\Omega_N), \tag{15}$$

recovers the fast convergence for the secular equation. In this case one finds that the eigenvalue E is invariant as H rotates. If E is real before the rotation, it remains real when H rotates. But this complex-rotation method enables us to include the open-channel segment with square-integrable basis functions. When we add the open-channel segment to the basis set ϕ_j, the total wave function becomes

$$\Psi(\mathbf{R}_N)=\sum_j C_j\phi(\mathbf{R}_N)+A\sum_{i,k} d_{ik}\psi_i(\mathbf{R}_{N-1})u_k(\mathbf{r}_N), \tag{16}$$

where C_j and d_{ik} are the linear parameters, and ψ_i are the open-channel target states. The angular coupling in Eq. (16) is suppressed. The u_k in Eq. (16) form a one-dimensional complete set. When H is complex scaled by an angle θ, Eq. (16) is also complex scaled as follows:

$$\Psi(R_Ne^{i\theta},\Omega_N)=\sum_j C_j\phi_j(R_Ne^{i\theta},\Omega_N)+A\sum_{i,k} d_{ik}\psi_i(R_{N-1}e^{i\theta},\Omega_{N-1})u_k(\mathbf{r}_n) \tag{17}$$

If we choose

$$u_k(r)=r^ke^{-\alpha r}, \tag{18}$$

the open-channel component becomes

$$\Psi_{open}=A\left[\sum_i\sum_{k=1}^{K_i} d_{ik}\psi_i(\mathbf{R}_{N-1})r_N^ke^{-\alpha_ir_N}Y_{l_Nm_N}(\mathbf{r}_N)\right]. \tag{19}$$

With this Ψ, the width and the shift are calculated from the secular equation

$$\delta\frac{\langle\Psi|H|\Psi\rangle}{\langle\Psi|\Psi\rangle}=0. \tag{20}$$

The real part of the eigenvalue gives us the resonance energy and the imaginary part gives the width of the resonance.

To achieve high accuracy, the basis functions should be able to saturate the functional space where the contribution to energy is significant. For nonorthogonal basis such as the Slater orbital used in this work, a large number of basis functions may lead to a linear dependence and numerical instability. To avoid this difficulty, we adopt the restricted variation method [22]. In this approach, the wave function of an atomic system is first solved with a smaller basis

$$\Psi_1(1,2,\ldots,N)=\sum_{i=1}^{I} C_i\phi_i(1,2,\ldots,N), \tag{21}$$

where I is the number of terms in the basis functions, and C_i's are the expansion coefficients determined by optimization. To improve this wave function with restricted variation method, we make a new expansion for the trial wave function

$$\Psi(1,2,\ldots,N)=D_1\Psi_1(1,2,\ldots,N)+\sum_{i=2}^{I'} D_i\psi_i(1,2,\ldots,N), \tag{22}$$

where ψ_i is linearly independent to at least one of the ϕ_i's in the wave function (21). The "basic function" (Ψ_1) is used as a single term in the variation calculation. The corresponding secular equation has the form

$$\det\begin{vmatrix} E_1-\lambda & H_{12}-\lambda S_{12} & H_{13}-\lambda S_{13} & \cdots & H_{1I}-\lambda S_{1I} \\ H_{21}-\lambda S_{21} & H_{22}-\lambda S_{22} & H_{23}-\lambda S_{23} & \cdots & H_{2I}-\lambda S_{2I} \\ \cdots & \cdots & \cdots & \cdots & \cdots \end{vmatrix}=0, \tag{23}$$

where

$$H_{1j}=\langle\Psi_1|H_0|\psi_j\rangle,\quad S_{1j}=\langle\Psi_1|\psi_j\rangle,\quad j=2,\ldots,I, \tag{24}$$

$$H_{ij}=\langle\psi_i|H_0|\psi_j\rangle,\quad S_{ij}=\langle\psi_i|\psi_j\rangle,\quad i,j=2,\ldots,I, \tag{25}$$

and λ is the eigenvalue. This secular equation is well behaved and an improved solution is obtained even if ψ_j is identical to part of the wave function in Ψ_1. In the restricted variation method, the entire Ψ_1 is reduced to a single term. New terms can be introduced quite liberally. The new secular equation is small and the computation can be done more quickly.

In this work, the photoionization cross section is calculated similar to Chung [13] based on a method suggested by Rescigno and McKoy [14] in which the PICS is obtained from the imaginary part of the polarizability. Highly accurate results have been obtained with this method [13]. The PICS is given by

$$\sigma(\omega)=\frac{4\pi^2}{3c}\omega\sum_{E_f=E_0+\omega}|\langle\Psi_0|\mathbf{D}|\Psi_f\rangle|^2 \tag{26}$$

where ω is the photon energy, $\mathbf{D}$ is the dipole operator, Ψ_0 is the initial ground-state wave function, and Ψ_f is the final-state wave function.

The polarizability of an atomic system is given by

$$\alpha(\omega)=\left(\sum_n\frac{|\langle\psi_0|\mathbf{D}|\Psi_n\rangle|^2}{E_n-E_0-\omega}+\int\frac{|\langle\psi_0|\mathbf{D}|\Psi_E\rangle|^2}{E-E_0-\omega-i\epsilon}dE+\sum_n\frac{|\langle\psi_0|\mathbf{D}|\Psi_n\rangle|^2}{E_n-E_0+\omega}\right)\Big/3. \tag{27}$$

Here we are interested in the negative-frequency part

$$\alpha_-(\omega)=\left(\sum_n\frac{|\langle\psi_0|\mathbf{D}|\Psi_n\rangle|^2}{E_n-E_0-\omega}+\int\frac{|\langle\psi_0|\mathbf{D}|\Psi_E\rangle|^2}{E-E_0-\omega-i\epsilon}dE\right)\Big/3, \tag{28}$$

and its imaginary component

$$\mathrm{Im}\,\alpha_-(\omega)=\tfrac{1}{2}\pi|\langle\Psi_0|\mathbf{D}|\Psi_f(E=E_0+\omega)\rangle|^2. \tag{29}$$

A comparison with Eq. (26) suggests that

$$\sigma(\omega)=\frac{4\pi\omega}{c}\mathrm{Im}\,\alpha_-(\omega). \tag{30}$$

$\alpha_-(\omega)$ may be obtained by first constructing a functional [23]

$$F=\langle\Psi_E|H_0-E_i-\omega|\Psi_E\rangle+\langle\Psi_0|D|\Psi_E\rangle+\langle\Psi_E|D|\Psi_0\rangle. \tag{31}$$

Ψ_E is then solved by finding the extremum for F after the complex scaling is done on Ψ_E. And finally, $\alpha_-(\omega)$ is given by the expression

$$\alpha_-(\omega)=\langle\Psi_E|D|\Psi_0\rangle/3. \tag{32}$$

III. RESULTS

In this study, a saddle-point method is used to calculate the singlet core-excited Be $1s2s2p^2\,{}^1S$, ${}^1D$, and ${}^1P$ resonances. These calculations have been carried out for the isoelectronic ions from Be I up to Ne VII.

In computing the energy of these four-electron states, we found that the radial and angular correlations are very important. To reach an accuracy comparable to that of two- and three-electron systems, much larger basis sets are needed. For each angular spin component, four nonlinear parameters are included for the Slater orbitals. They are optimized in the computation. An example of the calculated wave function and energy for the Be $1s2s2p^2\,{}^1S$ state is given in Table I. The spin wave functions χ^1 and χ^2 are given in Eq. (7).

The calculated energies (in a.u.) for the Be $1s2s2p^2\,{}^1S$, $1s2s2p^2\,{}^1D$, and $1s2s2p^2\,{}^1P$ together with the relativistic and mass polarization corrections are tabulated in Table II. Here E_0 is the energy obtained from the saddle-point method for the unperturbed Hamiltonian, Eq. (1). The perturbation corrections from each of the terms in Eq. (12) are listed with their contributions. The total correction E_1 are also given in this table. Most of the corrections come from the P4 (H_1) (the relativistic correction to the kinetic energy) and the Darwin term (H_2) [see Eq. (12)]. The expectation values of mass polarization (H_4) and the retardation potential effect (H_5) are opposite in sign. The energy shifts obtained from the complex-rotation calculation, ΔE_{shft}, and the correction from the restricted variation calculation, ΔE_{rsv}, are also given in this table. For the ${}^1S$ resonance, the energy shift is mainly due to the combination of two major decaying modes, that is, $1s2s2p^2\,{}^1S\rightarrow(1s^22s+e)$ and $1s2s2p^2\,{}^1S\rightarrow(1s^22p+e)$. Their branching ratios are listed in Table V, below. The resonance energy in the complex-rotation calculation is very stable over a wide range of θ and the nonlinear parameters α in Eq. (19). Up to $15u_k$'s are used. The real part of the energy is stable to about six or seven digits after the decimal. ΔE_{res} is the improvement of energy from the restricted variation method. In the case of Be $1s2s2p^2\,{}^1D$, an improvement of about 0.048 eV is obtained. The calculated energies for the core-excited BII and CIII resonances are given in Table III. The energies of the corresponding isoelectronic resonances for N IV, O V, F VI, and Ne VII are listed in Table IV. In this table, L_n is the number of partial waves and N is number of total basis terms.

Chung has studied the four-electron resonances of Be I and B II with the saddle-point method [16]. A larger basis set is utilized here which is further improved with the restricted variation calculation. Furthermore, we have employed the SPCR method to calculate the width, the energy shift, and the branching ratios for the decay channels. We noted that the energy shift obtained by SPCR is positive for ${}^1D$ and ${}^1S$ states, but is negative for ${}^1P$ state. The same pattern holds for all the iso-electron Be-like ions studied here.

The value for q represents the optimized effective charge seen by the vacancy orbital. The optimized values for ${}^1D$ or ${}^1S$ states is around $Z-0.5$, exhibiting the fact that the nuclear charge seen by the $1s$ vacancy is half-screened by the presence of the $1s$ electron. However, the shielding for

TABLE I. Energy (in 10^{-6} a.u.) and wave function for Be I $1s2s2p^2\,{}^1S$ ($q=3.42$). Here N is the number of basis functions. α_s are the nonlinear parameters.

$l_1l_2l_3l_4\chi$ [a]	$l_{12}l_{123}$	N	Energy	α_1	α_2	α_3	α_4
$0011\chi^2$	01	30	10 119 923.74	3.7546	1.5717	0.9279	1.7171
$0011\chi^1$	01	16	7105.39	3.8762	1.4710	1.8104	0.8449
$0022\chi^2$	02	30	19912.54	3.9551	0.8918	1.5147	1.6690
$0000\chi^2$	00	12	5404.69	3.9328	1.2966	0.4186	3.7847
$0033\chi^2$	03	8	1950.15	3.9274	0.7921	2.2305	2.0758
$0044\chi^2$	04	3	417.89	3.9668	1.0767	2.4731	2.9230
$0121\chi^2$	11	14	1858.90	4.0149	0.9388	1.6021	1.3359
$0022\chi^1$	02	8	20.46	3.9459	1.0802	1.8317	1.4135
$0121\chi^1$	11	14	1185.73	1.2025	1.0215	3.8021	3.2336
$0132\chi^2$	12	5	2932.58	3.9165	1.2260	1.7703	1.6510
$0231\chi^2$	21	5	545.23	3.8266	1.5948	2.1128	1.1952
$0132\chi^1$	12	5	273.98	3.8622	1.2177	2.0175	1.6203
$0121\chi^1$	11	14	246.83	3.9998	0.9828	1.5540	1.9309
$1111\chi^2$	01	4	737.27	2.6738	1.5637	0.7650	2.1590
$0101\chi^2$	11	34	1673.73	3.4951	1.0661	1.2105	1.8082
$0112\chi^2$	12	23	777.54	1.5941	0.9115	3.8954	3.4309
$0202\chi^2$	22	12	17.54	4.0140	1.3542	1.3461	1.7698
Total	17	237	10 164 984.21				

[a]The coupling scheme χ^1 and χ^2 are given in Eq. (7).

the ${}^1P$ states is more extensive. The q value of N IV $1s2s2p^2\,{}^1P$ is 6.07, indicating that the $2p$ electrons are pulled into the core by the strong nuclear charge. In this respect, it is interesting to notice the following distinction for the $1s2s2p^2\,{}^1P$ resonance: A simple consideration of Pauli's exclusive principle implies that the $1s2s2p2p\,{}^1L$ system may be formed through

$$(1s2s)^3S\,(2p2p)^3P\,{}^1P, \tag{33}$$

$$(1s2s)^1S\,(2p2p)^1D\,{}^1D, \tag{34}$$

$$(1s2s)^1S\,(2p2p)^1S\,{}^1S. \tag{35}$$

We list in Table V, Table VI, and Table VII the calculated branching ratios for the Auger electrons from $1s2s2p^2\,{}^1L$ for Be I, B II, and C III. The corresponding branching ratios for N IV, O V, F VI, and Ne VII are tabulated in Table VIII. Recently, Chung [21] used a spin-alignment dependent theory to explain the relative magnitude of the Auger branching ratios. It would be interesting to check this theory with our results. Most of the $1s2s2p^2\,{}^1L$ decay through both $1s^22s$ and $1s^22p$ channels. But because of parity violation, $1s2s2p^2\,{}^1P$ does not decay via the $1s^22s$ channel in the nonrelativistic approximation. For ions of low and median Z, the symmetry preferred decay may make the corresponding Auger lines particularly prominent in the observed Auger spectra.

For the $1s2s2p2p\,{}^1P$ resonances, two of the most probable decay channels are

TABLE II. Perturbation corrections and the energy shift for Be I $1s2s2p^2\,{}^1L$ resonances (in a.u.).

	$1s2s2p^2\,{}^1S$	$1s2s2p^2\,{}^1D$	$1s2s2p^2\,{}^1P$
q	3.42	3.46	3.16
E_0	−10.164 984	−10.238 362	−10.172 515
P4 and Darwin (H_1+H_2)	−0.001 895	−0.001 895	−001 963
e-e contact (H_3)	0.000 032	0.000 029	0.000 008
Mass polarization (H_4)	−0.000 017	−0.000 027	−000 029
Retardation potential (H_5)	0.000 029	0.000 025	0.000 015
E_1 (total correction)	−0.001 851	−0.001 868	−0.001 969
Subtotal	−10.166 835	−10.240 230	−10.174 484
ΔE_{shft}	0.001 018	0.000 665	−0.000 113
ΔE_{rsv}	−0.000 677	−0.001 751	−0.000 718
E_{total}	−10.166 826	−10.241 316	−10.175 315

TABLE III. Energies for the $1s2s2p^2$ singlet core-excited resonances of B II and C III (in a.u.).

Resonance	E_0	q	E_1	ΔE_{shft}	ΔE_{rsv}	E_{total}
B II $1s2s2p^2\,^1D$	−16.928 150	4.45	−0.004 742	0.001 070	−0.000 173	−16.931 995
B II $1s2s2p^2\,^1P$	−16.834 171	4.12	−0.004 966	−0.000 211	−0.000 508	−16.839 856
B II $1s2s2p^2\,^1S$	−16.831 844	4.46	−0.004 702	0.001 455	−0.000 305	−16.835 396
C III $1s2s2p^2\,^1D$	−25.370 121	5.45	−0.010 199	0.001 380	−0.000 181	−25.379 121
C III $1s2s2p^2\,^1P$	−25.248 451	5.11	−0.010 704	−0.000 285	−0.000 584	−25.260 024
C III $1s2s2p^2\,^1S$	−25.237 787	5.46	−0.010 097	0.002 054	−0.000 305	−25.246 135

$$1s2s2p2p\,^1P \rightarrow 1s1s2p + \epsilon p, \tag{36}$$

$$1s2s2p2p\,^1P \rightarrow 1s1s3p + \epsilon p. \tag{37}$$

In the initial states, the $1s$ electron and $2s$ electron form a triplet. The $2s$ cannot fall directly into the $1s$ vacancy. In the case of Eq. (36), the $1s$ vacancy is filled via a $2s-2p$ interaction either by a spin- or orbital-angular-momentum-exchanged electron. In the channel, Eq. (37), in addition to the this exchange, the other $2p$ electron needs to be further promoted to the $3p$ orbital. Thus, the probability for Eq. (37) is extremely small. This conclusion is supported by the calculated branching ratios.

For the $1s2s2p2p\,^1D$ resonances, the two major decaying modes are

$$1s2s2p2p\,^1D \rightarrow 1s1s2s + \epsilon d, \tag{38}$$

$$1s2s2p2p\,^1D \rightarrow 1s1s2p + \epsilon p. \tag{39}$$

Equation (38) may be considered as the result of interaction between the two $2p$ electrons such that one collapses to the $1s$ vacancy by changing angular momentum and the other leaves the atom as a free d electron. For Eq. (39), there are two possibilities. Both are the result of a $2s$ electron interacting with the nearest $2p$ electron. In the first case, the $2p$ electron collapses into the $1s$ vacancy, via the $2s$-$2p$ interaction and an angular momentum exchange. On the other hand, the $2s$ electron may fill the $1s$ vacancy without violating the exclusion principle since the $1s$ and the $2s$ electrons form a singlet in the initial state. The $2p$ electron will be kicked out as a free p electron. In this case, there is no need for angular momentum exchange. Hence, we expect the Eq. (39) would be the major contributor to the Auger transition. Our results support this conclusion.

For the $1s2s2p2p\,^1S$ resonance there are two major decay channels:

$$1s2s2p2p\,^1S \rightarrow 1s1s2s + \epsilon s, \tag{40}$$

$$1s2s2p2p\,^1S \rightarrow 1s1s2p + \epsilon p. \tag{41}$$

The situation is very similar to that of $1s2s2p2p\,^1D$ resonances and we conclude that the decay prefers the channel through (41). Our calculated branching ratios agree with this conclusion. In summary, our calculation support the spin-alignment-dependent theory proposed by Chung [21].

In the following subsections we will discuss our results for each ion and compare with available experimental and theoretical data in the literature.

A. Results for beryllium

The energy levels of Be for the states of interest are shown in Fig. 1. The calculated energies and the branching ratios for the Auger electrons of Be I $1s2s2p^2\,^1L$ resonances as well as the experimental results from the Be spectrum of Rødbro *et al.* [24] are tabulated in Table V. In this work, we use −14.326 897 a.u. for Be^+ $1s^22s$ from Ref.

TABLE IV. Energies of $1s2s2p^2$ states of N IV, O V, F VI, and Ne VII (in a.u.).

State		L_n	N	q	$-E_0$	$-E_1$	$-\Delta E_{shft}$	$-\Delta E_{rsv}$	$-E_{total}$
N IV	$1s2s2p^2\,^1D$	31	404	6.445	35.562 946	0.019 487	−0.001 625	0.002 640	35.583 448
	$1s2s2p^2\,^1P$	32	225	6.070	35.413 917	0.020 451	0.000 346	0.000 303	35.435 017
	$1s2s2p^2\,^1S$	25	318	6.452	35.397 621	0.019 319	−0.002 475	0.000 552	35.415 017
O V	$1s2s2p^2\,^1D$	31	404	7.443	47.506 253	0.034 092	−0.001 817	0.002 836	47.541 364
	$1s2s2p^2\,^1P$	32	225	7.000	47.329 749	0.035 759	0.000 400	0.000 355	47.366 263
	$1s2s2p^2\,^1S$	25	318	7.449	47.308 616	0.033 857	−0.002 803	0.000 593	47.340 263
F VI	$1s2s2p^2\,^1D$	31	404	8.448	61.201 952	0.055 891	−0.001 977	0.000 882	61.256 748
	$1s2s2p^2\,^1P$	32	225	7.940	60.995 850	0.058 436	0.000 448	0.000 278	61.055 012
	$1s2s2p^2\,^1S$	25	318	8.447	60.970 153	0.055 476	−0.003 064	0.000 630	61.023 195
Ne VII	$1s2s2p^2\,^1D$	31	404	9.442	76.645 840	0.086 839	−0.002 104	0.000 928	76.731 503
	$1s2s2p^2\,^1P$	32	225	8.841	76.412 118	0.090 520	0.000 487	0.000 309	76.503 434
	$1s2s2p^2\,^1S$	25	318	9.446	76.382 023	0.086 207	−0.003 278	0.000 429	76.465 381

TABLE V. Branching ratios (BR) of Be I $1s2s2p^2$ system for major decaying channels.

Channel	Energy (eV) Theory[a]	Chung[b]	Expt.[c]	BR[a]	Width (meV)[a]
$1s2s2p2p\,^1D \rightarrow 1s1s2s+\varepsilon d$	111.17			34.20%	12.41
$1s2s2p2p\,^1D \rightarrow 1s1s2p+\varepsilon p$	107.21	107.31	107.02±0.2	65.80%	23.89
Total width					36.97
$1s2s2p2p\,^1P \rightarrow 1s1s2p+\varepsilon p$	109.01	109.01	108.96±0.2	99.96%	4.813
$1s2s2p2p\,^1P \rightarrow 1s1s3p+\varepsilon p$	101.00		101.02±0.1	0.04%	0.002
Total width					4.958
$1s2s2p2p\,^1S \rightarrow 1s1s2s+\varepsilon s$	113.20			19.36%	5.940
$1s2s2p2p\,^1S \rightarrow 1s1s2p+\varepsilon p$	109.25	109.44	109.26±0.2	80.64%	24.74
Total width					30.48

[a]This work.
[b]Chung [16].
[c]Rødbro *et al.* [24].

[25] −14.181 546 a.u. for Be^+ $1s^22p$ from Ref. [26]. The results from Chung [16] are also listed for comparison.

The Be spectrum from Rødbro *et al.* [24] is shown in Fig. 2. In this spectrum, the lithiumlike $1s2l2l'$ lines are by far the most prominent. The spectral lines in the range 110–115 eV (lines 16–22) are shown to correspond to $1s2l3l'$ lithiumlike lines in Davis and Chung [28]. Lines 4, 5, 8, 9, 10, 11, 13, 14, and 15 which had not been identified in Ref. [28] were identified later in Ref. [16]. Using the energies in Fig. 1 and in Table V, we can reexamine these identifications.

Line 11 is weak but broad. The reported position is 107.02±0.2 eV. Our predicted result at 107.21 eV for the decay $1s2s2p^2\,^1D \rightarrow (1s^22p,e)$ is within the experimental uncertainty. The result in Davis and Chung [28], 107.32 eV, lies slightly outside the error bar.

Lines 14 and 15 are the most intense lines in the spectra. Line 14 appears as the strongest line at 108.96±0.2 eV in Fig. 2 and line 15 appears as a shoulder at 109.26±0.2 eV. Our calculation shows that they come from the following two transitions:

$$1s2s2p^2\,^1P \rightarrow (1s^22p,e) \text{ predicted at } 109.01 \text{ eV}, \quad (42)$$

$$1s2s2p^2\,^1S \rightarrow (1s^22p,e) \text{ predicted at } 109.25 \text{ eV}. \quad (43)$$

The calculated branching ratios in Table V show that both transitions (42) and (43) are the preferred decaying modes. The calculated results by Davis and Chung are 109.01 and 109.44 eV, respectively.

For the $1s2s2p^2\,^1D \rightarrow (1s^22s+e)$ channel, our predicted Auger energy is at 111.17 eV, buried in the lithiumlike lines. On the other hand, the spectral line due to the $1s2s2p^2\,^1P \rightarrow (1s^23p+e)$ transition is not plotted here for its extremely small branching ratio. If we use −13.887 158 a.u. for $1s^23p$, we obtain an Auger energy of 101.00 eV, within the experimental error bar of the weak line 4.

The channel $1s2s2p^2\,^1S \rightarrow (1s^22s+e)$ which was predicted to be 113.20 eV with relatively small branching ratio is not reported in the experiment.

TABLE VI. Auger energies and branching ratios for B II $1s2s2p^2\,^1D$, $1s2s2p^2\,^1P$ and $1s2s2p^2\,^1S$ resonances .

	Channel	Width (meV)	BR (%)	Auger energy (eV) Theory[a]	Chung[b]	Expt. (eV)[c]
	$1s^22s+d$	25.47	39.80	176.83	176.86	176.88±0.2
$1s2s2p^2\,^1D$	$1s^22p+p$	38.47	60.20	170.83	170.85	170.57±0.2
Total width		64.84				
	$1s^22p+d$	11.19	99.95	173.34	173.34	173.58±0.2
$1s2s2p^2\,^1P$	$1s^23p+p$	0.006	0.05	155.41		
Total width		11.19				
	$1s^22s+s$	19.60	35.57	179.46		
$1s2s2p^2\,^1S$	$1s^22p+p$	35.51	64.43	173.46	173.41	173.58±0.2
Total width		55.10				

[a]This work. For the $1s^22s$, $1s^22p$, and $1s^23p$ energies used, see text.
[b]Chung [16].
[c]Reference [29].

TABLE VII. Auger energies and branching ratios for C III $1s2s2p^2\,{}^1D$, $1s2s2p^2\,{}^1P$, and $1s2s2p^2\,{}^1S$ resonances.

	Channel	Width (meV)	BR (%)	Auger energy(eV)		
				E_e (eV) [a]	Theory	Expt.
	$1s^22s+d$	36.54	42.78	256.05	257.3 [b]	256.09 [c]
					255.3 [d]	256.1 [d]
$1s2s2p^2\,{}^1D$	$1s^22p+p$	48.87	57.22	248.05	247.2 [b]	248.04 [c]
						248.2 [d]
Total width		86.48				
	$1s^22p+d$	16.34	99.95	251.29	252.9 [b]	251.48±0.2 [c]
					252.8 [d]	251.4 [d]
$1s2s2p^2\,{}^1P$	$1s^23p+p$	0.008	0.05	219.60		
Total width		16.43				
	$1s^22s+s$	22.10	31.35	259.67	258.9 [d]	258.6 [d]
					260.9 [b]	259.99 [c]
$1s2s2p^2\,{}^1S$	$1s^22p+p$	48.40	68.65	251.67	252.8 [b]	251.48±0.2 [c]
					260.9 [d]	251.4 [d]
Total width		70.35				

[a]For the $1s^22s$, $1s^22p$, and $1s^23p$ energies used, see text.
[b]Chen, Ref. [32].
[c]Experimental results by Rødbro *et al.* [24] as recalibrated by Bruch *et al.* [30].
[d]Mann [31].

B. Results for boron

Our calculated energies, widths, and branching ratios for the B II $1s2s2p^2\,{}^1D$, $1s2s2p^2\,{}^1P$, and $1s2s2p^2\,{}^1S$ are shown in Table VI. For the energy of the Auger electrons, we use −23.430 622 a.u. for the $1s^22s$ [25], −23.210 334 a.u. for the $1s^22p$ [26], and −22.551 343 a.u. for the $1s^23p$ [27]. These results were obtained with the C I wave function including relativistic and mass polarization corrections. The experimental energy by Rødbro *et al.* [24] as recalibrated by Chung and Bruch [29] and the theoretical results by Chung [16] are also included in this table for comparison.

The Auger spectrum of boron by Rødbro *et al.* is reproduced in Fig. 3. The lithiumlike lines are unambiguously identified in Chung and Bruch [29]. These lines appear to have a higher intensity as compared with those of the four-electron spectral lines. The lines 9, 15, 16, and 18 with a very significant intensity have also been identified in Ref. [16]. Using the electron energies tabulated in Table VI, we can identify the possible lines for the $1s2s2p^2$ resonances.

Line 12 at 170.57±0.2 eV is a weak line. Our calculation shows that the observed line is $(1s2s2p^2\,{}^1D\rightarrow 1s^22p+e)$ predicted at 170.83 eV, in good agreement with the result 170.85 eV by Chung and the experiment.

Line 15 is reported at 173.58±0.2 eV with a strong intensity. We predict it to be the overlap of the following transitions:

$$1s2s2p^2\,{}^1P\rightarrow(1s^22p,e)\text{ predicted at 173.34 eV,}\quad(44)$$

$$1s2s2p^2\,{}^1S\rightarrow(1s^22p,e)\text{ predicted at 173.46 eV.}\quad(45)$$

These results are in agreement with the calculated results by Chung who obtained 173.34 eV and 173.41 eV, respectively. Equation (44) is a symmetry-preferred Auger decay. We notice that the other decay channel $1s2s2p^2\,{}^1S\rightarrow(1s^22s,e)$ predicted at 179.46 eV is not reported in the observed spectrum. This is also true in the reported C III and Be I Auger spectra. The calculated branching ratio of $1s2s2p^2\,{}^1S\rightarrow(1s^22s,e)$ is much smaller than $1s2s2p^2\,{}^1S\rightarrow(1s^22p,e)$.

Line 19 is reported at 176.88±0.2 eV. Our prediction for the channel $1s2s2p^2\,{}^1D\rightarrow(1s^22s,e)$ is 176.83 eV in good agreement with the result 176.86 eV in Ref. [16] and with the experiment. The branching ratios in Table VI show that the weak $1s2s2p^2\,{}^1D\rightarrow(1s^22p,e)$ is a preferred decaying mode as compared with the $1s2s2p^2\,{}^1D\rightarrow(1s^22s,e)$ channel. Hence, the latter one can not be the major contributor to line 19. Our calculations for boron are in complete agreement with Ref. [16].

C. Results for carbon

The energies, widths, and the branching ratios of C III $1s2s2p^2\,{}^1D$, $1s2s2p^2\,{}^1P$, and $1s2s2p^2\,{}^1S$ are shown In Table VII. For the energy of the Auger electrons we need the energies of the $1s^22s$, $1s^22p$, and $1s^23p$ ions. They are −34.789 074 a.u. for $1s^22s$ [25], −34.495 071 a.u. for $1s^22p$ [26], and −33.330 578 a.u. for $1s^23p$ [27].

Our calculated Auger energy for the core-excited singlet resonances of C III is compared with the experiment of Bruch *et al.* [30] which is recalibrated from Rødbro *et al.* [24]. The spectrum is reproduced in Fig. 4. In addition, we compare our results with the Auger spectra of Mann [31]. Note that the error bars in both experiments are ±0.2 eV.

Our predicted energy for the transition $1s2s2p^2\,{}^1D\rightarrow(1s^22p,e)$ is at 248.05 eV. This is in good agreement

TABLE VIII. Auger energies and branching ratios of N IV, O V, F VI, and Ne VII (in eV).

Channel		Energy (eV) [a]	BR [a]	Other Theo.	Expt.
N IV	$1s2s2p^2\,{}^1D\rightarrow 1s^22s+\varepsilon d$	348.84	44.67%		
	$1s2s2p^2\,{}^1D\rightarrow 1s^22s+\varepsilon p$	338.86	55.33%		
	$1s2s2p^2\,{}^1P\rightarrow 1s^22p+\varepsilon p$	342.90	99.95%		
	$1s2s2p^2\,{}^1P\rightarrow 1s^23p+\varepsilon p$	293.63	0.05%		
	$1s2s2p^2\,{}^1S\rightarrow 1s^22s+\varepsilon s$	353.42	30.48%		
	$1s2s2p^2\,{}^1S\rightarrow 1s^22p+\varepsilon p$	343.44	69.52%		
O V	$1s2s2p^2\,{}^1D\rightarrow 1s^22s+\varepsilon d$	455.35	46.00%	456.74[b], 455.4[c]	457 ± 2[c]
	$1s2s2p^2\,{}^1D\rightarrow 1s^22p+\varepsilon p$	443.36	54.00%	444.65[b], 443.4[c]	444 ± 1[c]
	$1s2s2p^2\,{}^1P\rightarrow 1s^22p+\varepsilon p$	448.13	99.96%	449.89 [b]	448.5 ± 1[c]
	$1s2s2p^2\,{}^1P\rightarrow 1s^23p+\varepsilon p$	377.51	0.04%		
	$1s2s2p^2\,{}^1S\rightarrow 1s^22s+\varepsilon d$	460.83	30.28%	462.10[b], 461.3[c]	460 ± 2[c]
	$1s2s2p^2\,{}^1S\rightarrow 1s^22p+\varepsilon p$	448.83	69.72%	450.01[b], 449.3[c]	449 ± 1[c]
F VI	$1s2s2p^2\,{}^1D\rightarrow 1s^22s+\varepsilon d$	575.55	46.93%		
	$1s2s2p^2\,{}^1D\rightarrow 1s^22p+\varepsilon p$	561.55	53.07%		
	$1s2s2p^2\,{}^1P\rightarrow 1s^22p+\varepsilon p$	567.04	99.96%		
	$1s2s2p^2\,{}^1P\rightarrow 1s^23p+\varepsilon p$	471.27	0.04%		
	$1s2s2p^2\,{}^1S\rightarrow 1s^22s+\varepsilon d$	581.91	30.29%		
	$1s2s2p^2\,{}^1S\rightarrow 1s^22p+\varepsilon p$	567.91	69.71%		
Ne VII	$1s2s2p^2\,{}^1D\rightarrow 1s^22s+\varepsilon d$	709.46	47.73%	710.84[d], 709.21[e]	710.0 ± 0.4[f]
	$1s2s2p^2\,{}^1D\rightarrow 1s^22p+\varepsilon p$	693.43	58.27%	694.71[d], 693.18[e]	694.0 ± 0.4[f]
	$1s2s2p^2\,{}^1P\rightarrow 1s^22p+\varepsilon p$	699.64	99.97%	701.42[d]	
	$1s2s2p^2\,{}^1P\rightarrow 1s^23p+\varepsilon p$	574.91	0.03%		
	$1s2s2p^2\,{}^1S\rightarrow 1s^22s+\varepsilon d$	716.71	30.38%	717.96[d], 716.57[e]	
	$1s2s2p^2\,{}^1S\rightarrow 1s^22p+\varepsilon p$	700.68	69.62%	701.83[d], 700.54[e]	

[a]This work. For the $1s^22s$, $1s^22p$, and $1s^23p$ energies used, see text.
[b]Reference [33].
[c]Reference [34].
[d]Multiconfiguration Dirac-Fock method [35].
[e]$1/Z$ method [36].
[f]Reference [36].

with Line 14 in Ref. [30] at 248.04 eV and with line 13 in Ref. [31] at 248.2 eV. This line overlaps with the three-electron line $1s2p^2\,{}^1S\rightarrow(1s^2,e)$ at 248.02 ± 0.2 eV. Note that line 13 in Ref. [33] is a very strong peak.

The most intense line reported in the spectrum of Ref. [30] is line 16 at 251.48 ± 0.2 eV. It is reported at 251.4 ± 0.2 eV in Mann. Our results show that it could be a overlap of

$$1s2s2p^2\,{}^1P\rightarrow 1s^22p+e \text{ predicted at } 251.29 \text{ eV}, \quad (46)$$

$$1s2s2p^2\,{}^1S\rightarrow 1s^22p+e \text{ predicted at } 251.67 \text{ eV}, \quad (47)$$

which all agree well with the observed peak. The calculated branching ratios in Table VII show that both transitions (46) and (47) are the favored decay modes. This may help to explain the strong intensity of this observed line.

Line 20 is reported at 256.09 eV in Ref. [30] and 256.1 ± 0.2 eV in Mann [31]. Our predicted energy for the channel $1s2s2p^2\,{}^1D\rightarrow(1s^22s+e)$, 256.05 eV, agrees very well with both experiments.

Our predicted energy at 259.07 eV for $1s2s2p^2\,{}^1S\rightarrow(1s^22s+e)$ deviates from line 19 at 258.6 eV or line 20 at 261.6 eV in the experiment of [31]. However, it agrees very well with line 25 at 259.02 eV in the experiment of Ref. [30]. The branching ratios between the decay modes of $(1s^22p,e)$ and $(1s^22s,e)$ is about 2:1. If the former mode is observed with significant intensity, the decaying mode $1s2s2p^2\,{}^1S\rightarrow(1s^22s+e)$ should also be observable. This is confirmed by our agreement with the experiment [30].

D. Results for O and Ne

We list in Table IV the calculated energies for the core-excited $1s2s2p^2\,{}^1L$ resonances and the branching ratios for the isoelectronic N IV, O V, F VI, and Ne VII ions.

Our Auger electron energy for O V $1s2s2p^2\,{}^1D\rightarrow(1s^22s+e)$ is 455.35 eV. It is 456.74 eV in Ref. [35] and 455.4 eV in Ref. [34]. These values are in agreement with the 457 ± 2 eV (line 7) in the experiment [34]. Our predicted Auger energy for $1s2s2p^2\,{}^1D\rightarrow(1s^22p+e)$ at 443.36 eV is close to the 444.65 eV in Ref. [33] and 443.4 eV in Ref. [34]. The experimental line 5′ at 444 ± 1 eV from Ref. [34] is a good candidate for this decay.

For the Auger energies of $1s2s2p^2\,{}^1S\rightarrow(1s^22p+e)$ and $1s2s2p^2\,{}^1S\rightarrow(1s^22s+e)$, we obtained 460.83 and 448.83

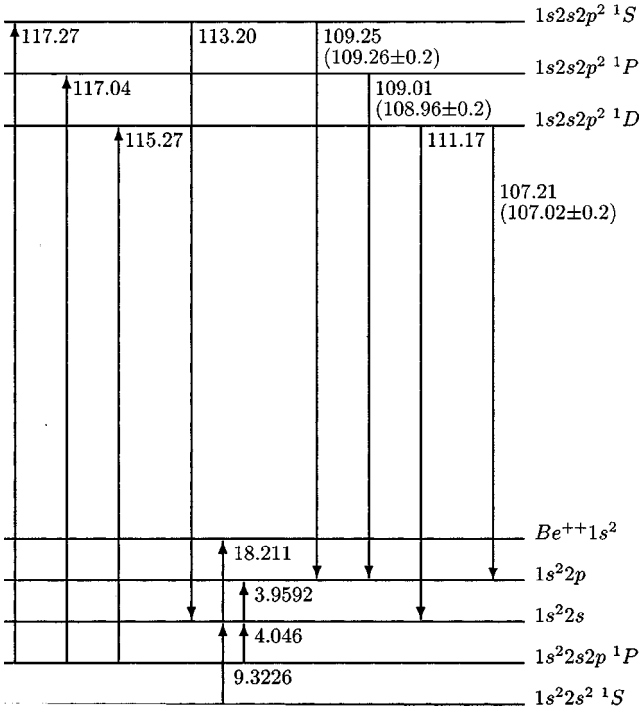

FIG. 1. Energy levels of Be (in eV). Numbers inside brackets denote the experimental data from Rødbro *et al.* [24].

eV, respectively. They are 462.10 and 450.01 eV in Ref. [33] and 461.3 and 449.3 eV in Ref. [34]. The experimental values 460 ± 2 eV of line $8'$ and 449 ± 1 eV of line $8'$ from Ref. [34] agree well with these predictions.

Our result 448.13 eV for O V $1s2s2p^2\,^1P\rightarrow(1s^22p+e)$ is close to the 449.89 eV from Ref. [33]. These values are very close to the line 448.5 ± 1 eV in the experiment [34]. The corresponding channel to $(1s^23p+e)$ is weak. It is not reported. In general, the agreements with the available theoretical and experimental data are good.

Our results for Ne VII are compared with the ones obtained from the $1/Z$ method, from Multiconfiguration Dirac-Fock (MCDF) method [35], and with experiment [35]. The experimental spectrum is reproduced in Fig. 5.

Our calculated energy for the channels $1s2s2p^2\,^1D\rightarrow(1s^22s+e)$ and $1s2s2p^2\,^1D\rightarrow(1s^22p+e)$ are at 693.43 and 709.46 eV, respectively. These results lie slightly lower

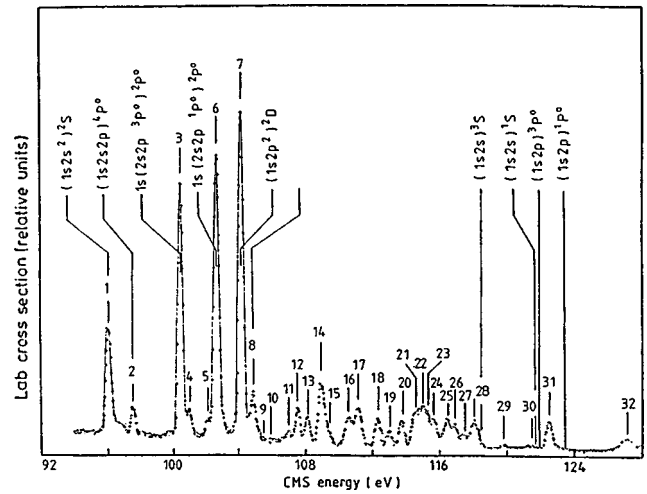

FIG. 2. Auger spectrum of Be with a singly excited core (500 keV on CH_4). Experimental data from Rødbro *et al.* [24].

the error bars of line B9a at 694.0 ± 0.4 eV and line B12 at 710.0 ± 0.4 eV in Fig. 5. Our energies are slightly higher than the 693.18 and 709.21 eV from the $1/Z$ method but are lower than the 694.71 and 710.84 eV from the MCDF method. For the decay $1s2s2p^2\,^1S\rightarrow(1s^22s+e)$, our predicted energy is 716.71 eV as compared with the 717.96 eV from the MCDF method and the 716.57 eV from $1/Z$ method. Our predicted energy for the corresponding $(1s^22p+e)$ channel is 700.68 eV. The calculated results from the MCDF method and from the $1/Z$ method are 701.83 eV and 700.54 eV, respectively. Our predicted energy is 699.64 eV for $1s2s2p^2\,^1P\rightarrow(1s^22p+e)$ decay. It is within the error bars of both lines C10 at 699.3 ± 0.4 eV and B10 at 699.8 ± 0.4 eV in Ref. [35].

IV. RESULTS FOR BERYLLIUM PHOTOIONIZATION RESONANCES

An energy diagram for Be autoionization and photoionization is shown in Fig. 1. The photon energies required for the transitions $1s^2s2p\,^1P+h\nu\rightarrow1s2s2p^2\,^1S$, ^1P, and ^1D are indicated in this figure. The calculated PIC'S for $1s^22s2p\,^1P^o$ near the ^1D resonance are shown in Fig. 6. These PICS's are obtained from Eq. (26). The Ψ_0 in Eq. (26)

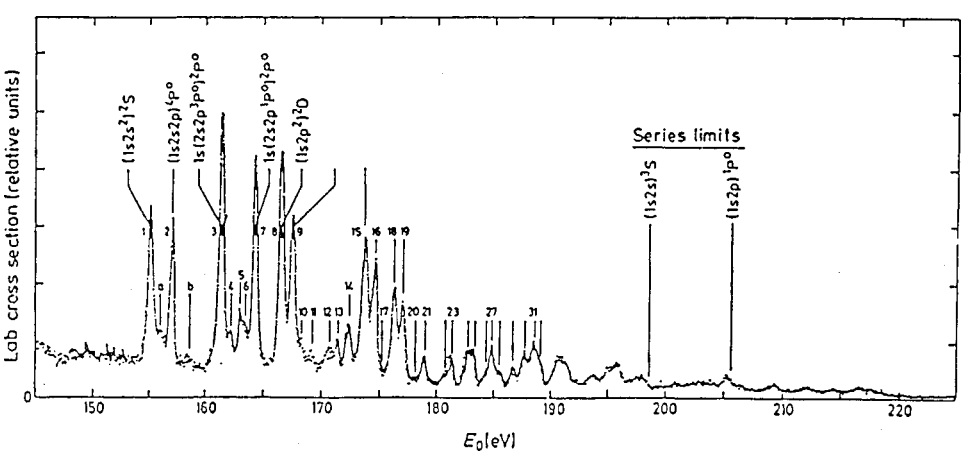

FIG. 3. Singly core-excited B Auger spectrum from 300 keV B^+ on CH_4. Experimental data from Rødbro *et al.* [24].

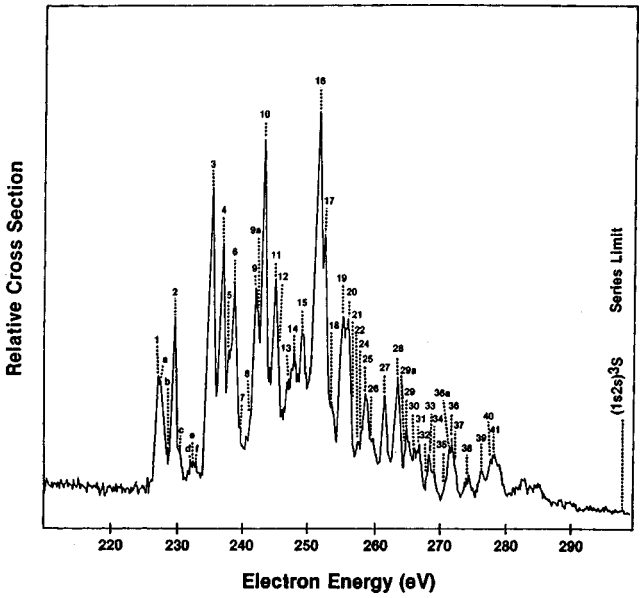

FIG. 4. High-resolution *KLL* Auger spectrum from Ref. [24]. 300 keV C^+ on CH_4.

is the Be I $1s^2 2s2p\,^1P^o$ state. We have used full-core plus correlation (FCPC) method to calculate the energy and wave function of this state. For the final state, we have

$$\Psi_f = A\left(\sum_o \Phi_0(1,2,3)\psi_o(4)\right) + \Psi_c(1,2,3,4)$$

where Φ_0 are the Be^+ $1s^2 2s$ and $1s^2 2p$ wave functions. An important criterion for the wave function Ψ_c is that it must

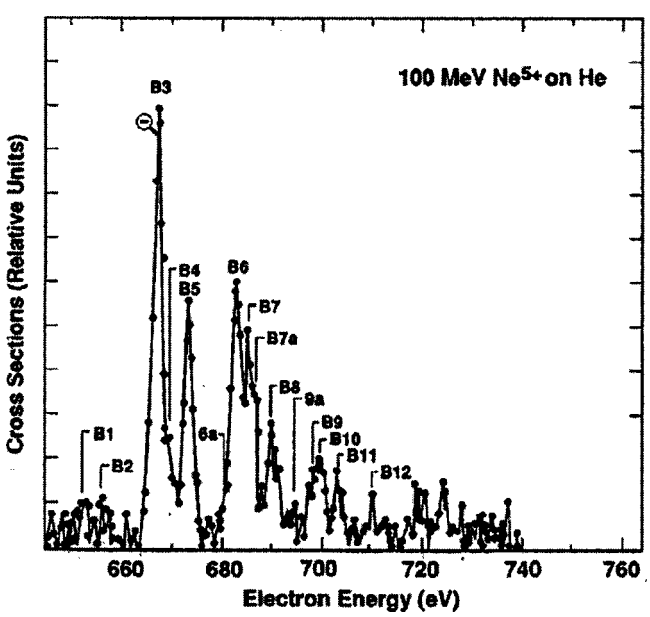

FIG. 5. High-resolution zero-degree electron spectrum produced by 100-MeV Ne^{5+} + He collisions. The spectrum is displayed after background subtraction and transformation to the projectile rest frame. The observed Auger lines arise mainly from Be-like core-excited $1s2s^2 2p$ and $1s2s2p^2$ initial configurations. (see also Ref. [36]).

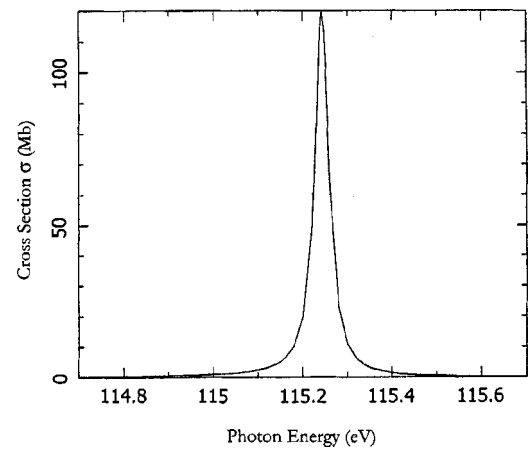

FIG. 6. Beryllium $1s2s2p^2\,^1D$ resonance from $1s^2 2s2p\,^1P^o$.

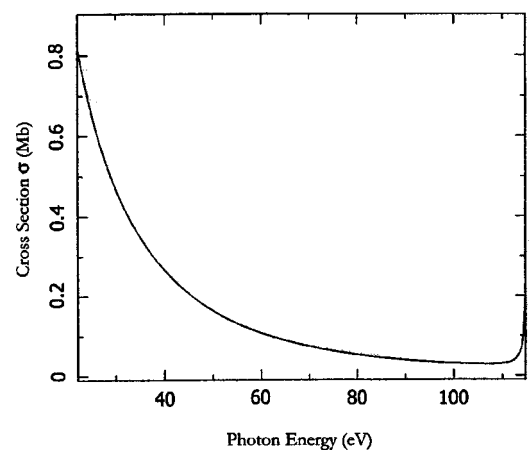

FIG. 7. Beryllium photoionization from $1s^2 2s2p\,^1P^o$, near the ^1D nonresonant region.

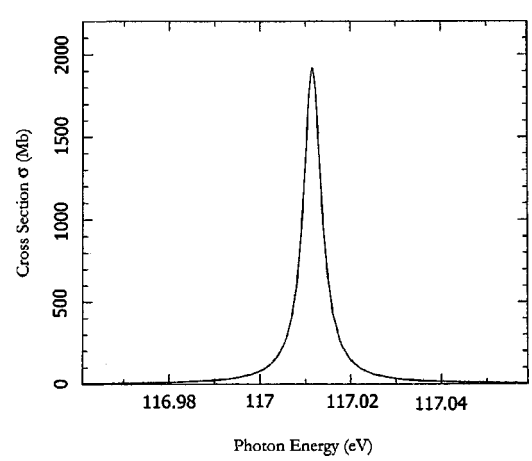

FIG. 8. Beryllium $1s2s2p^2\,^1P$ resonance from $1s^2 2s2p\,^1P^o$.

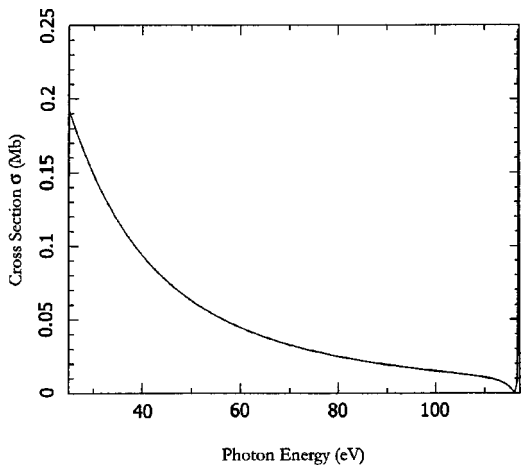

FIG. 9. Be photoionization from $1s^2 2s2p\,^1P^o$, near the ^1P nonresonant region.

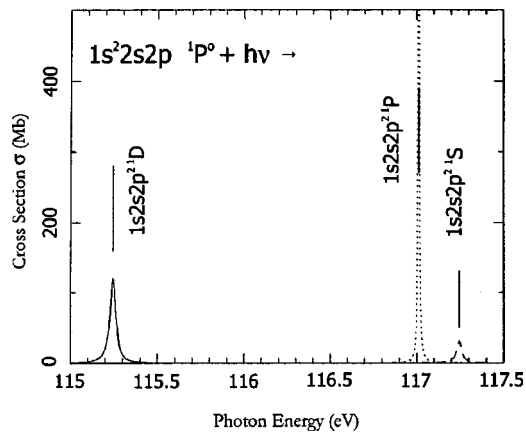

FIG. 12. Be photoionization from $1s^2 2s2p\,^1P^o$.

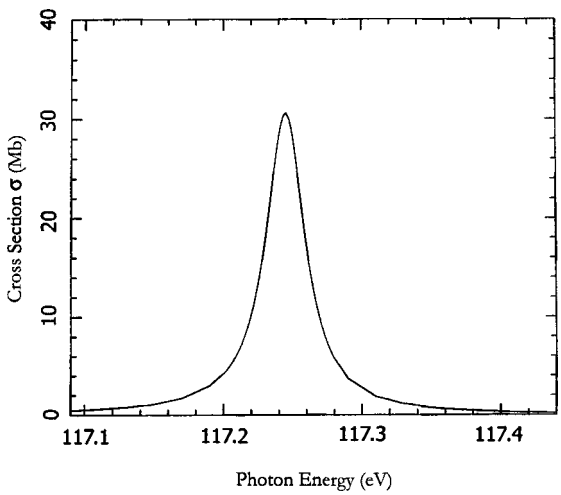

FIG. 10. Beryllium $1s2s2p^2\,^1S$ resonance from $1s^2 2s2p\,^1P^o$.

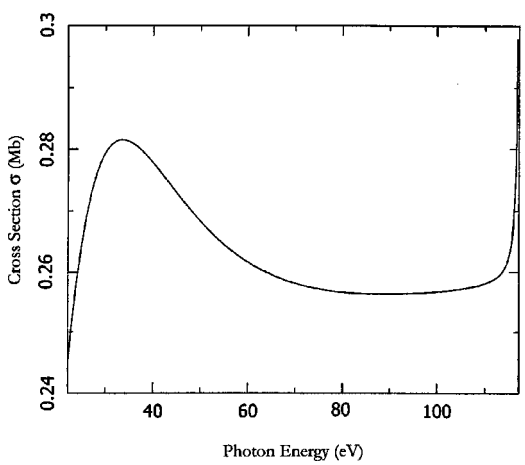

FIG. 11. Beryllium photoionization $1s^2 2s2p\,^1P^o$, near the ^1S nonresonant region.

give the energy of the resonances in this region accurately without spurious singularity. The peak cross section of this resonance is at around 120 Mb (1.2×10^{-16} cm^2).

In Fig. 7, the same PICS calculation in the nonresonant region for Be I $1s^2 2s2p\,^1P^o + h\nu \rightarrow {}^1D$ is shown. Notice that the value of the largest cross section is around 0.8 Mb, 150 times smaller than the peak in the resonant region.

In Fig. 8, we show the calculated cross section in the resonant region for Be $1s^2 2s2p\,^1P^o + h\nu \rightarrow 1s2s2p^2\,^1P$. The peak cross section in this region is at around 1900 Mb. We show the same PICS's in the nonresonant region in Fig. 9. Again, the value of the largest cross section is about 10 000 times smaller than the resonant region.

The cross section in the resonant region for Be $1s^2 2s2p\,^1P^o + h\nu \rightarrow Be\,1s2s2p^2\,^1S$ is presented in Fig. 10. The peak cross section is at approximately 30 Mb. The corresponding cross section in the nonresonant region is presented in Fig. 11. Here, the value of the largest cross section is about 100 times smaller than the peak cross section in the resonant region. The total PICS's predicted for Be from $1s^2 2s2p\,^1P^o$ are given in Fig. 12.

V. CONCLUSION

In this work, we have computed the Auger energies from Be-like $1s2s2p^2\,^1L$ systems for $Z=4$–10. The PICS's for Be I $1s^2 2s2p\,^1P^o$ are calculated for the first time. Most of the predicted energies lie inside the quoted experimental error bars. For some of the unresolved lines in the experiments, we hope our results could be helpful to identify them. They should be useful in future experimental analysis as well for ions from Be I to Ne VII.

Although our results agree well with experiments, it should be noted that our relativistic corrections are obtained with first-order perturbation theory. This theory, while accurate for small-Z systems, will become less accurate as Z increases.

ACKNOWLEDGMENTS

This work is supported by Grant No. NSC 89-2112-M007-008 of National Science Council of Taiwan, ROC and by National Science Foundation Grant No. PHY 00-70431. This work was started while K.T.C. was visiting the National Center for Theoretical Sciences at Tsing-Hua University He was also supported by National Science Council of Taiwan, Republic of China.

[1] L. M. Kiernan, M.-K. Lee, B. F. Sonntag, P. Sladeczek, P. Zimmermann, E. T. Kennedy, J-P. Mosnier, and J. T. Costello, J. Phys. B **28**, L161 (1995).
[2] Y. Azuma, S. Hasegawa, F. Koike, G. Kutluk, T. Nagata, E. Shigemasa, A. Yagishita, and I. A. Sellin, Phys. Rev. Lett. **74**, 3768 (1995).
[3] L. Journel, D. Cubaynes, J.-M. Bizau, S. Al Moussalami, B. Rouvellou, F. J. Wuilleumier, L. VoKy, P. Faucher, and A. Hibbert, Phys. Rev. Lett. **76**, 30 (1996).
[4] S. Diehl, D. Cubaynes, J.-M. Bizau, L. Journel, B. Rouvellou, S. Al Moussalami, F. J. Wuilleumier, E. T. Kennedy, N. Berrah, C. Blancard, T. J. Morgan, J. Bozek, A. S. Schlachter, L. VoKy, P. Faucher, and A. Hibbert, Phys. Rev. Lett. **76**, 3915 (1996).
[5] X. Yang, C. G. Bao, and C. D. Lin, Phys. Rev. Lett. **76**, 3096 (1996).
[6] S. Diehl *et al.*, Phys. Rev. A **56**, R1071 (1997).
[7] Y. Azuma, F. Kolke, J. W. Cooper, T. Nagata, E. Shigemasa, R. Wehlitz, and I. A. Sellin, Phys. Rev. Lett. **79**, 2419 (1997).
[8] M. Meyer, B. Müller, A. Nunnemann, Th. Prescher, E. v. Raven, M. Richter, M. Schmidt, B. Sonntag, and P. Zimmermann, Phys. Rev. Lett. **59**, 2963 (1987).
[9] D. Cubaynes *et al.*, Phys. Rev. Lett. **77**, 2194 (1996).
[10] S. Bashkin and J. O. Stoner, Jr., *Atomic Energy Levels and Grotrian Diagrams II* (Elsevier, New York, 1975).
[11] K. T. Chung, Phys. Rev. A **20**, 1743 (1979).
[12] K. T. Chung and B. F. Davis, Phys. Rev. A **26**, 3278 (1982).
[13] K. T. Chung, Phys. Rev. Lett. **78**, 1416 (1997); Phys. Rev. A **56**, R3330 (1997).
[14] T. N. Rescigno and V. McKoy, Phys. Rev. A **12**, 522 (1975).
[15] K. T. Chung and B. F. Davis, in *Autoionization-Recent Developments and Applications*, edited by A. Temkin (Plenum, New York, 1985), Chap. 3; B. F. Davis and K. T. Chung, Phys. Rev. A **37**, 111 (1988); B. Jaskoslka and W. Woznicki, Phys. Scr. **39**, 230 (1989).
[16] K. T. Chung, J. Phys. B **23**, 2929 (1990).
[17] K. T. Chung, Phys. Scr. **42**, 530 (1990).
[18] K. T. Chung, Phys. Scr. **42**, 537 (1990).
[19] K. T. Chung, Phys. Rev. A **42**, 645 (1990).
[20] K. T. Chung, Chin. J. Phys. (Taipei) **27**, 507 (1989).
[21] K. T. Chung, Phys. Rev. A **59**, 2065 (1999).
[22] K. T. Chung and X. W. Zhu, Phys. Scr. **48**, 292 (1993).
[23] A. Dalgarno and J. T. Lewis, Proc. R. Soc. London, Ser. A **48**, 233 (1955).
[24] M. Rødbro, R. Bruch, and P. Bisgaard, J. Phys. B **12**, 2413 (1979).
[25] K. T. Chung, Phys. Rev. A **44**, 5421 (1991).
[26] K. T. Chung and X.-W. Zhu, Phys. Scr. **48**, 292 (1993).
[27] Z.-W. Wang, X.-W. Zhu, and K. T. Chung, Phys. Scr. **47**, 65 (1993).
[28] B. F. Davis and K. T. Chung, J. Phys. B **15**, 3113 (1982).
[29] K. T. Chung and R. Bruch, Phys. Rev. A **28**, 1418 (1983).
[30] R. Bruch, K. T. Chung, W. L. Luken, and J. C. Culberson, Phys. Rev. A **31**, 310 (1985).
[31] R. Mann, Phys. Rev. A **35**, 4988 (1987).
[32] M. H. Chen, At. Data Nucl. Data Tables **34**, 301 (1986).
[33] M. H. Chen, Phys. Rev. A **31**, 1449 (1985).
[34] R. Bruch, D. Schneider, W. H. E. Schwarz, M. Meinhart, B. M. Johnson, and K. Taulbjerg, Phys. Rev. A **19**, 587 (1979).
[35] R. Bruch, D. Schneider, M. H. Chen, K. T. Chung, and B. F. Davis, Phys. Rev. A **44**, 5659 (1991).
[36] A. Itoh, D. Schneider, T. Schneider, T. J. M. Zouros, G. Nolte, G. Schiweietz, W. Zeitz, and N. Stolterfoht, Phys. Rev. A **31**, 684 (1985).